metals

MDPI

Review

Design, Fabrication, and Characterization of New Materials Based on Zirconia Doped with Mixed Rare Earth Oxides: Review and First Experimental Results

Adrian Mihail Motoc [1,*], Sorina Valsan [1,*], Anca Elena Slobozeanu [1,*], Mircea Corban [1], Daniele Valerini [2,*], Mythili Prakasam [3], Mihail Botan [4], Valentin Dragut [1], Bogdan St. Vasile [5], Adrian Vasile Surdu [5], Roxana Trusca [5], Maria Luisa Grilli [6,*] and Robert Radu Piticescu [1,*]

1 National R&D Institute for Nonferrous and Rare Metals-IMNR, Laboratory for Advanced and Nanostructured Materials and HighPTMET Center, 102 Biruintei Blvd, Pantelimon, 077145 Ilfov, Romania; corban.mircea@imnr.ro (M.C.); dragutv@imnr.ro (V.D.)
2 ENEA–Italian National Agency for New Technologies, Energy and Sustainable Economic Development, Brindisi Research Centre, S.S.7 Appia-km 706, 72100 Brindisi, Italy
3 University Bordeaux, CNRS, Bordeaux INP, ICMCB, UMR 5026 Pessac, 33600 Bordeaux, France; mythili.prakasam@ubordeaux.fr
4 National R&D Institute for Aeronautics "Elie Carafoli", 066126 Bucharest, Romania; botan.mihail@incas.ro
5 National Research Center for Micro and Nanomaterials, University Politehnica from Bucharest, 060042 Bucharest, Romania; bogdan.vasile@upb.ro (B.S.V.); adrian.surdu@upb.ro (A.V.S.); roxanatrusca@yahoo.com (R.T.)
6 ENEA-Italian National Agency for New Technologies, Energy and Sustainable Economic Development, Casaccia Research Centre, Via Anguillarese 301, 00123 Rome, Italy
* Correspondence: amotoc@imnr.ro (A.M.M.); svalsan@imnr.ro (S.V.); a.slobozeanu@imnr.ro (A.E.S.); daniele.valerini@enea.it (D.V.); marialuisa.grilli@enea.it (M.L.G.); rpiticescu@imnr.ro (R.R.P.); Tel.: +402-135-220-48 (A.M.M.)

Received: 29 April 2020; Accepted: 29 May 2020; Published: 3 June 2020

Abstract: Monazite is one of the most valuable natural resources for rare earth oxides (REOs) used as dopants with high added value in ceramic materials for extreme environments applications. The complexity of the separation process in individual REOs, due to their similar electronic configuration and physical–chemical properties, is reflected in products with high price and high environmental footprint. During last years, there was an increasing interest for using different mixtures of REOs as dopants for high temperature ceramics, in particular for ZrO_2-based thermal barrier coatings (TBCs) used in aeronautics and energy co-generation. The use of mixed REOs may increase the working temperature of the TBCs due to the formation of tetragonal and cubic solid solutions with higher melting temperatures, avoiding grain size coarsening due to interface segregation, enhancing its ionic conductivity and sinterability. The thermal stability of the coatings may be further improved by using rare earth zirconates with perovskite or pyrochlore structures having no phase transitions before melting. Within this research framework, firstly we present a review analysis about results reported in the literature so far about the use of ZrO_2 ceramics doped with mixed REOs for high temperature applications. Then, preliminary results about TBCs fabricated by electron beam evaporation starting from mixed REOs simulating the real composition as occurring in monazite source minerals are reported. This novel recipe for ZrO_2-based TBCs, if optimized, may lead to better materials with lower costs and lower environmental impact, as a result of the elimination of REOs extraction and separation in individual lanthanides. Preliminary results on the compositional, microstructure, morphological, and thermal properties of the tested materials are reported.

Keywords: zirconia; rare earth zirconates; thermal barrier coatings; microstructure characterization; thermal shock resistance

1. Introduction

Necessity for better performance and efficiency in applications across stationary power plants, aerospace and automotive industries has led to the development of thermal barrier coatings (TBCs) and multi-layer coating systems over the last 50 years [1]. During recent years it was demonstrated that co-doping of zirconia ceramics with rare earth oxides (REOs) may avoid grain size coarsening due to interface segregation, enhancing its ionic conductivity and sinterability [2,3]. The co-doping of zirconia with different REOs was reported to improve the thermal properties of thermal barrier coatings and oxidation properties due to reduction of mechanical stresses and porosity in the oxide layers [4,5]. These improvements play a crucial role in the segments mentioned above because they are effective means for protecting the hot parts against the effects of high temperature in corrosive/erosive environments, extending the life of the metallic parts and reducing the maintenance costs [6–9].

Typically, TBCs are made up of different successive layers deposited on a substrate (typically made of a super alloy): the metal bond coat (BC), the thermally-grown oxide (TGO) generated at the interface by oxidation of the bonding layer, and the upper layer (top coat) in direct contact with the environment [10]. In order to operate under extreme conditions, an effective TBC must meet certain requirements, which severely limits the number of materials that can be used. Low thermal conductivity, high melting point, phase stability, good adhesion to the substrate, chemical inertia, thermodynamic compatibility with the metallic substrate and TGO, high thermal cycling resistance are the major requirements to be achieved [6,11].

Ceramic materials are usually capable of satisfying the required properties. Compared to metallic materials, ceramic coatings offer several advantages due to the high hardness and wear resistance when exposed to thermal and corrosive conditions, coupled with relatively low densities [12]. Flame-sprayed Al_2O_3/CaO-doped ZrO_2 ceramic coatings were firstly developed. However, they did not prove to be viable materials for the more advanced thermal barrier applications due to relatively high thermal conductivity and phase transitions of Al_2O_3, leading to shrinkage and the associated cracking effect on coating life [7,13].

Yttria-doped zirconia (ZrO_2 doped with 7–8 wt.% Y_2O_3) are presently considered as a "gold standard" in coating materials for TBC applications [14]. Compared to other ceramics, zirconia has good corrosion / erosion resistance, lower intrinsic thermal conductivity and a coefficient of thermal expansion best suited [6]. Table 1 illustrates some important properties of the traditional TBC layers.

Table 1. Properties of thermal barrier coatings (TBC).

TBC Properties		
Al_2O_3 (TGO)	NiCoCrAlY	8YSZ
T_m ~2323 K λ = 5.8 W m^{-1}·K^{-1} (1400 K) α = 9.6 × 10^{-6} K^{-1} (1273 K) E = 30 GPa (293 K) υ = 0.26	T_m ~1863 K λ = 320 W m^{-1}·K^{-1} (293 K) α = 10.7 × 10^{-6} K^{-1} (293–1273 K) E = 40 GPa (293 K) υ = 0.22	T_m ~2873 K λ~2.5 W m^{-1}·K^{-1} (298 K) α = 10.7 × 10^{-6} K^{-1} (293–1273 K) E = 40 GPa (293 K) υ = 0.22

Symbols in the table have the following meanings: TGO—thermally grown oxide on bond coat; T_m—melting point; λ—thermal conductivity; α—thermal expansion coefficient; E—Young's modulus; υ—Poisson's number.

The stable form of pure ZrO_2 is the monoclinic phase, present at temperatures below 1100 °C. Between 1100 and 2370 °C ZrO_2 crystallizes in the tetragonal phase, and the cubic phase is found between 2370 °C and 2706 °C (the melting point) [14,15]. The mechanical properties of zirconia are

drastically affected by microcracking caused by the transition from the tetragonal to the monoclinic phase, which occurs with an increase in volume of about 4%. Dopants such as MgO, CaO, Y_2O_3, and other rare earth oxides are compulsory to stabilize both the tetragonal and cubic phases at room temperature [6,15]. These ceramic materials have very broad and interesting range of electrical, mechanical, thermal, optical and biocompatibility properties, which result from the structural and the intrinsic chemical-physical properties listed in Table 1 [15]. Y_2O_3-stabilized ZrO_2 (YSZ) was found to be the most suitable material for TBC applications, with an optimum amount of Y_2O_3 around 7–8 wt.% (4–4.5 mol%). This composition offers a high degree of resistance to spallation and excellent thermal stability as presented in Table 2 [16,17].

Table 2. ZrO_2 properties [16].

ZrO_2 Properties			
Melting point, °C	2700	Evaporation rate μm/h × 10^{-5} at 1650 °C	670
Density, g/cm^3	5.6	at 1927 °C	0.75
Vapor pressure, Pa × 10^{-6} at 1650 °C	10.6	at 2200 °C	44
×10^{-5} at 1927 °C	127	Oxygen permeability g/cm^{-1} s^{-1} × 10^{-13} at 1000 °C	120
×10^{-3} at 2200 °C	78.7	×10^{-11} at 1400 °C	60
Crystal structure below 1170 °C	Monoclinic	×10^{-10} at 1800 °C	30
1170–2370 °C	Tetragonal	Limit of stability with carbon, °C	1600
2370–2706 °C	Cubic	Thermal expansion, ppm/°C	7.5

However, at temperatures above 1200 °C in the long term, YSZ loses its phase stability but the main critical issue is calcium–magnesium–alumino–silicate (CMAS) attack that lowers the thermal insulating power [18,19]. Therefore, it is desired to develop new TBCs that can operate at a temperature above 1200 °C. An actual research topic is doping ZrO_2 ceramics with different rare earth oxides due to their high temperature transformation and the low thermal conductivity, which allow to increase the operating temperatures of turbines.

2. Synthesis and Properties of ZrO_2 Ceramic Powders Doped with Mixed REOs

Different methods were proposed for the synthesis of zirconia doped with mixed rare earth oxides. We report in the following about different synthesis routes, the different ZrO_2 dopants and different applications, with focus on TBCs.

ZrO_2 thin films doped with 8 wt.% rare earths (Ce, Gd, and Y) were prepared by Sasikumar et al. on glass substrates by sol-gel, followed by spin-coating technique and annealed at 600 °C. X-ray diffraction (XRD) analysis revealed that for non-doped ZrO_2 films, only the monoclinic phase is present, while for the doped ZrO_2 films both monoclinic and tetragonal phase appear. Because of doping with RE ions, the crystallite size decreased with the increase of oxygen vacancies. Scanning electron microscopy (SEM) images exhibited the rod-shaped and square-shaped grains for the undoped ZrO_2 and Gd:ZrO_2 thin films, respectively [20].

Ce-doped ZrO_2 and Dy-doped ZrO_2 were synthesized by Mekala and co-workers by a coprecipitation method. The XRD study revealed that the synthesized nanoparticles showed tetragonal (t-ZrO_2) and monoclinic (m-ZrO_2) phase and also confirmed the decrease in crystal size with Dy and Ce doping. Apparently, doping with RE had different effects on the size and morphology of ZrO_2 nanopowders. ZrO_2 doped with Ce had the smallest particle size (6 nm), doping with Dy led to particle size of 9 nm, and the non-doped ZrO_2 size was about 12 nm. Authors stated that Ce doped sample has nano-flakes like morphology, Dy doping has snow-flakes like morphology and undoped has cauliflower-like morphology. This result reveals that Dy doping promotes, and Ce doping inhibits the grain growth and crystallization of ZrO_2, which was consistent with the result of XRD analysis [21].

To understand the thermal behavior of redox ability for different ceria-zirconia based materials during thermal aging process, Deng and collaborators have sintered five CeO_2–ZrO_2–Y_2O_3–La_2O_3 quaternary mixed oxides (CZ) with varied ratio of Ce/Zr. The Ce-rich CeO_2–ZrO_2 based oxide

(Ce/Zr >1) exhibits a declined oxygen storage capacity (OSC) and deteriorated reducibility after thermal aging. Raman and X-Ray Photoelectron Spectroscopy (XPS) analyses suggest that the abundant available Zr ions in Zr-rich samples do not incorporate into ceria lattices completely during moderate calcination, and that these remaining Zr ions migrate into ceria lattices further during thermal aging accompanied by sintering. This is considered as the most reasonable explanation for the enhanced OSC of Zr-rich samples after thermal aging [22].

ZrO_2 powders doped with 9.5% Y_2O_3, 5.6% Yb_2O_3, and 5.2% Gd_2O_3 have been synthesized by a chemical co-precipitation method with improved thermal stability at 1300 °C for 50 h. The higher phase's stability was given by the increased concentration of stabilizers leading to the increase of the concentration of oxygen vacancies, thus decreasing the tetragonality [14].

Madhusudhana et al. synthesized Gd (1–9 mol%) doped ZrO_2 nanocrystals by solution combustion method using Glycine as a fuel, furnace temperature being 400 °C. XRD analysis showed high crystallinity of the sample, with particle size of 25–35 nm. It was observed that the addition of Gd^{3+} ions influences the change of the structure of ZrO_2 grains from flaky structures at 1 mol% of Gd, to uniform spherical structures at 9 mol% of Gd, creating more oxygen vacancies. AC impedance spectroscopy results of the as synthesized Gd doped ZrO_2 show good dielectric properties with a very high dielectric constant ($\varepsilon' = 345$) and as well a high AC conductivity ($\sigma_{ac} = 0.06837$ S·cm^{-1}) at 10 MHz for 7 mol% of Gd doped ZrO_2. This material is best suitable for solid oxide fuel cell applications [23].

Xiao and co-workers systematically investigated the band gap, the interfacial properties and the optoelectronic properties of Gd (0.5, 10, 15 mol%) doped ZrO_2 high-k gate dielectric films deposited by solution method, reaching the conclusion that the incorporation of Gd has a positive effect on optimizing ZrO_2 dielectrics applied in further Complementary Metal Oxide Semiconductor (CMOS) devices. They found that the band gap of sample increases with the increase of Gd concentration, conduction band offset increases from 2.57 to 3.06 eV with the increase of Gd concentration, indicating that the band offset is larger than the minimum requirement for the barrier height of over 1 eV for future CMOS. The increase of dielectric constant (k) from 8.5 to 10.3 with the Gd concentration increase from 0 to 10% may be attributed to the Gd incorporation, which is favorable for improving the interfacial quality and prevent the growth of low-k SiOx interlayer. When the Gd concentration increases to 15%, the k value decreases, which is probably due to the lower dielectric constant of Gd_2O_3 comparing with ZrO_2. The negative flat-band voltage values suggest that there are positive oxide charges in the film, which may be attributed to the oxygen vacancies and positive fixed charges in the film and near the interface. The incorporation of Gd also decreases leakage current density from 3.2×10^{-5} to 1.8×10^{-6} A/cm^2 [24].

Lei Guo and co-workers fabricated by co-precipitation and calcination method 1 mol% RE_2O_3 (RE = La, Nd, Gd, and Yb) and 1 mol% Yb_2O_3 co-doped YSZ (1RE1Yb-YSZ), in order to obtain improved phase stability and reduced thermal conductivity. For 1RE1Yb-YSZ ceramics, the phase stability of the metastable tetragonal phase (t') increased with decreasing size of RE^{3+}, mainly attributed to the reduced driving force for the partitioning of the t' phase. By codoping, the thermal conductivity was lower than that of YSZ, with the exception of the sample 1La1Yb-YSZ, which showed an undesirable high thermal conductivity, being attributable to the high content of phase m due to the decomposition of phase t'. Authors stated that, considering the full ceramic properties, 1Gd1Yb-YSZ could be a good potential material for TBC applications [25].

In their study, Xiwen Song et al. investigated the influences of the partial substitution of Y_2O_3 with the equivalent Ln_2O_3 (Ln = Nd, Sm, and Gd) on the phase structure and thermal properties of ZrO_2–Nb_2O_5–Y_2O_3 ceramics. The powders for ZrO_2–Nb_2O_5–Y_2O_3–Ln_2O_3 samples were synthesized by solid-state reaction of well-mixed stable oxides. All ZrO_2–Nb_2O_5–Y_2O_3–Ln_2O_3 compositions consist of a single non-transformable tetragonal phase with an exceptionally high tetragonality. However, partial replacement of Y^{3+} with Ln^{3+} results in a slight decrease in tetragonality. These compositions have low thermal conductivity. The composition with Nd^{3+} replaced with Y^{3+} showed

the lowest thermal conductivity of ~1.69 W m^{-1} K^{-1}, approximately 30% lower than that of composition ZrO_2–Nb_2O_5–Y_2O_3 [26].

Xiwen Song and co-workers determined the effect of rare earth oxides Ln_2O_3 (Ln = Nd, Sm, and Gd) on the structure and thermal properties of ZrO_2-based ceramics doped with 8.3 mol% Ta_2O_5 + 8.3 mol% Y_2O_3 by solid-state reaction. When 1 mol% Ln_2O_3 substituted 1 mol% Y_2O_3, all composites showed only the tetragonal phase. The results of the study suggest that the addition of Ln_2O_3 may be a viable strategy for decreasing grain growth, specific heat capacity and thermal conductivity, which is beneficial in improving the performance of the ZrO_2–Ta_2O_5–Y_2O_3 system for TBC applications. The most effective oxide in reducing the thermal conductivity of the system was Gd_2O_3 [27].

Mikhailov and al. obtained fine-grained ceramics based on solid solutions of ZrO_2–x–Ln_2O_3 (where Ln = Sm and Yb). These were obtained by the colloidal chemical synthesis of the powders followed by SPS (spark plasma sintering). They showed that the addition of lanthanides in zirconium efficiently stabilizes the structure and no phase transformation occurs during heating, ensuring a high density of the ceramic obtained by SPS and high hydrolytic stability. They also demonstrated that the introduction of lanthanides leads to a higher intensity of contraction and reduces the activation energy of ceramic sintering based on ZrO_2. The influence of lanthanide oxides on the sintering activation energy of ceramics in SPS is determined by the influence of ions of Sm^{3+} and Yb^{3+} on the diffusion properties of grain boundaries and by the proportion between the atom radius of zirconium and lanthanides [28].

Bahamirian developed a new material, ZGYbY powder: $ZrO_2$9.5$Y_2O_3$5.6$Yb_2O_3$5.2Gd_2O_3 synthesized by the chemical precipitation method, in order to increase the stability of the YSZ phases at higher temperatures. During the thermal cycle at 1100 °C for 50 h they confirmed the stability of the phases of both powders, ZGYbY and YSZ. The results of the thermal cycle at 1300 °C for 50 h indicated that the YSZ powder decomposed into two new phases, including cubic and monoclinic zirconia, while the ZGYbY powder exhibited excellent stability due to the complete retention of the t' zirconia phase and the transition from tetragonal to monoclinic phase upon cooling. These results make ZGYbY a promising material for TBC applications [13].

YiTao Wang and coworkers obtained by solid state reactions x mol% ZrO_2-Gd_3NbO_7 dense ceramics (x = 0, 3, 6, 9, 12), a promising candidate for TBC applications. The ZrO_2-Gd_3NbO_7 ceramic showed only orthorhombic crystal structures with uniform grain size, ranging from 2 to 20 μm. The thermal conductivity of ZrO_2-Gd_3NbO_7 is much lower, 1.21–1.82 (W·m^{-1}·K^{-1}) from 25 to 900 °C, compared to $La_2Zr_2O_7$ (1.50–2.00 W·m^{-1}·K^{-1}), Y_2SiO_5, 8YSZ (2.50–3.00 W·m^{-1}·K^{-1}), ZrO_2-Eu_3TaO_7, ZrO_2-$DyTaO_4$, ZrO_2-Y_2O_3-Ta_2O_5 and YbO. The thermal expansion coefficients (TEC) for ZrO_2-Gd_3NbO_7 range from 9.71–10.60 × 10^{-6} K^{-1} (1200 °C), being higher than those of $La_2Zr_2O_7$ (9.00 × 10^6 K^{-1}), La_2SiO_5 (6.90–8.80 × 10^{-6} K^{-1}) and YSZ (10.00 × 10^{-6} K^{-1}). The mechanical properties of Gd_3NbO_7 change slightly with increasing ZrO_2 content, Vickers hardness was about 10 GPa, and Young's modulus was 173–195 GPa, which was lower than YSZ (240 GPa). A lower Young's modulus results in materials with lower stiffness [29].

Chao Chen et al. investigated the effect of Sc_2O_3 in YSZ ceramics on hot corrosion behavior in molten salts Na_2SO_4 + V_2O_5 (50/50 wt.%) at 1000 °C. By chemical coprecipitation method followed by calcination they obtained powders of xSc_2O_3−1.5Y_2O_3-ZrO_2 (x = 4.5, 5.5, 6.5, in mol%) and 4.5 mol% Y_2O_3-ZrO_2, and compared their properties. They noted that with increasing Sc_2O_3 content, corrosion resistance and phase stability also increase. On the surface of the YSZ ceramic, corroded bar-shaped configuration appears, while it turns into granular shapes with reduced amounts when higher Sc_2O_3 was used to dope YSZ. Introduction of Sc_2O_3 into YSZ can enhance the M-O bond strength and the substrate's ability to prohibit vanadate penetration due to the relatively shorter ionic radius of Sc^{3+} than that of Y^{3+} and Zr^{4+}. Furthermore, the least possibility to react Sc_2O_3 with V_2O_5, according to the Gibbs free energy calculation and the Lewis acid-base rule, promotes the phase stability of the ScYSZ

ceramics. The excellent hot corrosion resistance can be achieved for those ScYSZ ceramics with higher Sc_2O_3 content, such as $6.5Sc_{1.5}$YSZ [30].

ZrO_2-$YO_{1.5}$-$TaO_{2.5}$ powders were prepared by Pitek et al. by inverse co-precipitation of mixed solutions of precursor salts and showed improved phase stability, corrosion resistance by sulfate/vanadate melting and resistance at least comparable to that of the reference 7YSZ material. The 16.6%$YO_{1.5}$ + 16.6%$TaO_{2.5}$ stabilized zirconia composition is tetragonal, stable against phase partitioning up to at least 1500 °C, and insensitive to the tetragonal–monoclinic transformation upon thermal cycling. This material also showed only slight evidence of corrosion in S/V melts after 500 h, compared with extensive attack and spallation at much shorter times (50–100 h) observed in 7YSZ [31].

In their work, Fan and colleagues studied the reduction mechanism in thermal conductivity of a series of Sc_2O_3-Y_2O_3 co-stabilized tetragonal ZrO_2 ceramics, finding a thermal conductivity that is 20–28% lower than zirconia stabilized with 6–8 wt.% of Y [32].

Sun at al. studied the phase stability and thermo-physical properties of 7.5 mol% Sc_2O_3 and Gd_2O_3 co-doped ZrO_2 (ScGdSZ). They stated that after 150 h heat treatment at 1400 °C, there was no monoclinic phase in Sc_2O_3 and Gd_2O_3 co-doped ZrO_2, indicating high phase stability of ScGdSZ. The substitution of Sc_2O_3 with Gd_2O_3 resulted in increased fraction of cubic phase, however, t′ phase was still the dominant phase when the substitution amount was less than 2 mol%. They noticed that with increasing the Gd_2O_3 proportion the thermal conductivity of ScGdSZ gradually decreased, owing to the larger cation radius and heavier atomic mass of Gd^{3+}. 3.7 Sc_2O_3 and 3.7 Gd_2O_3 co-doped ZrO_2 (in mol%) had the lowest thermal conductivity, which was 20% lower than 7.5 ScSZ and 40% lower than 4.5 YSZ, respectively [33]. Table 3 summarizes the influence of the synthesis route on the structure and morphology of ZrO_2 doped with mixed rare earth oxides.

Table 3. The structural and morphological properties of the different materials based on ZrO_2 doped with rare earth oxides.

Nr.	Material	Technique	Structural and Morphological Properties	Reference
1	8 wt.% rare earth (Ce, Gd and Y) doped ZrO_2 films	sol-gel	monoclinic and tetragonal phases; doping with RE ions, the crystallite size is reduced (D = 6752 nm for ZrO_2 undoped, D = 4640 nm for doped ZrO2).	[20]
2	Ce doped ZrO_2, Dy doped ZrO_2	coprecipitation	tetragonal and monoclinic phases; doping with RE ions, the crystallite size is reduced (D = 12 nm for ZrO_2 undoped, D = 9 nm for ZrO_2/Dy, D = 6 nm ZrO_2/Ce).	[21]
3	(Gd (1–9 mol%) doped ZrO_2	solution combustion	D = 25–35 nm	[23]
4	1 mol% RE_2O_3 (RE = La, Nd, Gd, Yb)	by co-precipitation	tetragonal phase	[25]
5	partial substitution of Y_2O_3 with the equivalent Ln_2O_3 (Ln = Nd, Sm, Gd) in ZrO_2-Nb_2O_5-Y_2O_3 ceramics	-	tetragonal phase	[25]
6	ZrO_2-doped with (8.3% mol Ta_2O_5 + 8.3% molY_2O_3 by solid-state reaction.-1 mol.% Ln_2O_3 substituted 1 mol% Y_2O_3	solid-state reaction	decreasing grain growth	[27]
7	ZrO_2-x-Ln_2O_3 (where Ln = Sm, Yb)	colloidal chemical synthesis	no phase transformation occurs during heating	[28]
8	ZrO_2 9.5Y_2O_3 5.6Yb_2O_3 5.2Gd_2O_3	chemical precipitation	excellent stability of tetragonal phase (of the thermal cycle at 1300 °C for 50 h)	[13]
9	*x* mol% ZrO_2-Gd_3NbO_7 dense ceramics (x = 0, 3, 6, 9, 12)	solid state reactions	D = 2–20 μm	[29]
10	*x*Sc_2O_3–1.5Y_2O_3-ZrO_2 (*x* = 4.5, 5.5, 6.5, in mol%)	chemical coprecipitation	increasing Sc_2O_3 content, phase stability also increases.	[30]
11	ZrO_2-$YO_{1.5}$-$TaO_{2.5}$	co-precipitation	tetragonal phase	[31]

Table 4 summarizes the solid phase expected to exist in ZrO_2-Y_2O_3-Ln_2O_3 systems in thermal equilibrium conditions, based on the analysis of the corresponding thermal phase diagrams, assessing the mutual compatibility between YSZ and corresponding zirconates.

Table 4. Equilibrium compounds in the ternary diagrams ZrO_2–Y_2O_3–Ln_2O_3 (where Ln = Gd_2O_3, Sm_2O_3, CeO_2, La_2O_3, and Nd_2O_3).

Material	T [°C]	Compounds Present in the Ternary Diagram	Reference
ZrO_2–Y_2O_3–Gd_2O_3	1200	F = fluorite; C = bixbyite; T = tetragonal ZrO_2; P = pyrochlore $Gd_2Zr_2O_7$; δ = $Y_4Zr_3O_{12}$	[34]
	1400	F = fluorite; C = bixbyite; T = tetragonal ZrO_2; P = pyrochlore $Gd_2Zr_2O_7$; β = B-Gd_2O_3	
	1600	F = fluorite; C = bixbyite; T = tetragonal ZrO_2; β = B-Gd_2O_3	
ZrO_2–Y_2O_3–Sm_2O_3	1250 1400 1600	F = cubic (fluorite structure) $(Zr_{1-x}(Y,Sm)x)O_{2-0.5x}$ ss; T = tetragonal $(Zr_{1-x}(Y,Sm)_x)O_{2-0.5x}$ ss; Pyr = $(Sm,Y)_2Zr_2O_7$ss (pyrochlore); B = monoclinic $(Sm,Y)_2O_3$ ss; C = cubic $(Y,Sm)_2O_3$ ss.	[35]
ZrO_2–Y_2O_3–CeO_2	1250	T = tetragonal; F = cubic fluorite; C = cubic; δ = $Zr_3(Y_{1-x}Ce_x)_4O_{12}$.	[36]
	1400	Tss = tetragonal solid solution; Fss = fluorite-type solid solution; Css = body-centered cubic solid solution.	[37]
	1600	Tss = tetragonal zirconia structure; Css = cubic fluorite structure; Yss = C-type yttria structure.	[38]
ZrO_2–Y_2O_3–La_2O_3	1250	A = hexagonal A-La_2O_3; B = monoclinic phase; C = cubic phase; F = fluorite phase; LaYP = $La_2Y_2O_6$ pyrochlore phase; Pyr = La–Y–Zr phase.	[39]
	1400	A = hexagonal A-La_2O_3; B = monoclinic phase; C = cubic phase; F = fluorite phase; LaYP = $La_2Y_2O_6$ pyrochlore phase; Pyr = La–Y–Zr phase.	
	1600	A =hexagonal A-La_2O_3; B = monoclinic phase; C = cubic phase; F = fluorite phase; LaYP = $La_2Y_2O_6$ pyrochlore phase; Pyr = La–Y–Zr phase.	
ZrO_2–Y_2O_3–Nd_2O_3	1250 1400 1600	A = RE hexagonal solid solution; B = RE monoclinic solid solution; C = RE cubic solid solution; solution; F = cubic fluorite solid solution; T = trigonal solid solution; Pyr = $Nd_2Zr_2O_7$ pyrochlore.	[40]

3. REO-Doped ZrO_2-Based Thermal Barrier Coatings

Coatings obtained from YSZ powder co-doped with Gd and Yb synthesized by hydrothermal method have also shown a higher thermal insulation capacity than the YSZ coatings [18]. YSZ ceramics co-doped with Gd and Yb produced by co-precipitation and calcination exhibit a better corrosion resistance than YSZ [10]. LZ/YSZ double-layer coating has a higher strength and oxidation resistance. LZ prevents the rapid oxidation of bondcoat and the rapid growth of thermal grown oxide (TGO). La^{3+} reduces the residual stress because it can control the phase transformation of TGO, by reducing the transition rate from the metastable phase θ-Al_2O_3 to the stable phase α-Al_2O_3 [16].

Zirconia stabilized with $x$$Sc_2O_3$–20 mol% CeO_2 (x = 3.6, 4.78, 5.63, 6.31, and 8 mol%) were successfully synthesized and the resistance to thermal shock was studied. After heat treatment at 1400 °C for 25 h, the results showed that the optimum structure was obtained for x = 4.78 due to avoding the formation of monoclinic and cubic phases in the structure of the stable tetragonal phase (t') [41].

Erbia-doped YSZ coatings fabricated by electron beam evaporation develop thicker oxide layers upon oxidation that lower even further their thermal diffusivity (conductivity) [42].

Rare-earth zirconates with perovskite or pyrochlore structure are presently considered as emerging TBC materials for the future. These pyrochlore phases are stable up to the melting point (around 2300 °C), making those potential TBC materials for higher application temperatures. They also have a low intrinsic thermal conductivity, associated with the complexity of crystallographic structure and difference in the number and types of atoms in a unit cell. At 1000 °C, the thermal conductivities are 1.5–1.6 $W{\cdot}m^{-1}{\cdot}K^{-1}$ and 1.2–1.3 $W{\cdot}m^{-1}{\cdot}K^{-1}$ for dense $La_2Zr_2O_7$ (LZO) and $Nd_2Zr_2O_7$, respectively. At 700 °C, the thermal conductivity values range from 1.5 to 1.6 $W{\cdot}m^{-1}{\cdot}K^{-1}$ for dense $Gd_2Zr_2O_7$ (GZO), $Nd_2Zr_2O_7$ (NZO), and $Sm_2Zr_2O_7$ (SZO) compared to 2.3 $W{\cdot}m^{-1}{\cdot}K^{-1}$ for dense 7YSZ [5]. The low thermal conductivity property comes from the fact that its pyrochloral structure ($A_2B_2O_7$) produces large quantities of oxygen ion vacancies and from the ionic mass difference between La^{3+} and Zr^{4+} which results in the phonon scattering [42,43]. Previous work has indicated that LZO exists in a single stable phase of pyrochloride up to its melting point (~2300 °C). Although LZO is considered a promising candidate for application as thermal barrier coatings due to its properties, its fracture toughness (0.9–1.3 $MPa{\cdot}m^{0.5}$) is lower than that of YSZ (~3 $MPa{\cdot}m^{0.5}$) [44,45]. Also, the lower coefficient of thermal expansion (CTE) of LZO may increase the mismatch stress in TBCs system during thermal cycling [46,47]. Below are presented the results of several studies that considered the use of LZO as a material for TBC.

Five different TBC systems, YSZ, $La_2Zr_2O_7$, $Gd_2Zr_2O_7$, YSZ/$La_2Zr_2O_7$, and YSZ/$Gd_2Zr_2O_7$, were produced and exposed to furnace thermal cyclic oxidation tests. The deposition of protective ceramic top coats was performed with Electron-Beam Physical Vapor Deposition (EB–PVD), single-layer coatings having a thickness of approximately 200 µm, while the thickness of each two-layer coating was approximately 100 µm. It was found that TBC double layers have a higher lifetime compared to TBCs with single layer. As a result of the performed cycling tests, the best performance was exhibited by the YSZ/$Gd_2Zr_2O_7$ coating system whereas $La_2Zr_2O_7$ TBC system displayed the lowest performance [48].

To prove the effect of the $La_2Zr_2O_7$ layer deposited on the YSZ layer on the thermal conductivity and oxygen penetration, two systems were exposed to isothermal and thermal cyclic oxidation tests. The two systems, YSZ and YSZ/$La_2Zr_2O_7$ top coats were deposited using EB–PVD technique. The stress distribution showed that the YSZ/LZ system has a longer life span than the YSZ TBC. Although the oxidation and thermal cyclic tests showed that double layer YSZ/LZ TBC exhibited better performance than single layer YSZ TBC, there is no drastic difference between the thermal performances of TBCs [49].

Another study suggested the use of $La_2Zr_2O_7$ in the design of TBC, for its low thermal conductivity. Although YSZ has been used as a top coat for TBC due to its thermal diffusivity, the major disadvantage of its use is its limited long-term operating temperature. Thus, two systems of functional graded coatings were obtained based on Al_2O_3/$La_2Zr_2O_7$/YSZ ceramics: a five-layer system (Al_2O_3/75%Al_2O_3 + 25%$La_2Zr_2O_7$/25%Al_2O_3 + 25%YSZ + 50%$La_2Zr_2O_7$/50%YSZ + 50%$La_2Zr_2O_7$/75%YSZ + 25%$La_2Zr_2O_7$) and a six-layer system (Al_2O_3/75%Al_2O_3 + 25%$La_2Zr_2O_7$/25%Al_2O_3 + 25%YSZ + 50%$La_2Zr_2O_7$/50%YSZ + 50%$La_2Zr_2O_7$/75%YSZ + 25%$La_2Zr_2O_7$/100% YSZ), using atmospheric plasma spray technique (APS). The researchers used alumina directly as a starting layer, near the metal substrate, because it acts as an oxygen diffusion barrier that protects the metal substrate from oxidation. $La_2Zr_2O_7$ powder was prepared using the sol-gel technique. It was found that samples coated with YSZ over 75% YSZ + 25% $La_2Zr_2O_7$ possess higher resistance to the attack of a Na_2SO_4 + V_2O_5 molten mixture up to 50 h of treatment than those coated with 75%YSZ + 25% $La_2Zr_2O_7$ top coats [50].

A comparison was made between YSZ as a conventional ceramic top coating material, Gd_2Zr_2O and YSZ/Gd_2Zr_2O as new generation coating materials with rare earth zirconate content. These materials were deposited as ceramic top coatings with EB–PVD method onto the CoNiCrAlY bond coat. These samples were subjected to hot corrosion tests by spreading mixtures of 55% V_2O_5 and 45% Na_2SO_4 salt at 5 h intervals at 1000 °C. It turned out that double coatings of YSZ/$Gd_2Zr_2O_7$ proved to be more resistant to hot corrosion than other single coatings [51].

YSZ/$Gd_2Zr_2O_7$ system was developed by the APS technique. Plasma grade flowable 8 wt.% YSZ and GZO powders were prepared by a single step co-precipitation technique. FE–SEM cross-section analysis of the YSZ/GZO bilayer coating after corrosion test demonstrated the effectiveness of the bilayer design in preventing the penetration of corrosive salts to the YSZ layer. Also, YSZ/GZO bilayer TBC exhibited a higher thermal cyclic life (300 cycles) than the single layer 8YSZ (175 cycles) coatings at 1100 °C [52].

Besides the above mentioned and commonly employed techniques for the fabrication of zirconia-based thermal barrier coatings, namely EB–PVD and plasma spraying (PS), also the sputtering technique is sometimes used to fabricated TBCs, especially in combination with the other techniques. Sputter-deposited films can provide good insulating properties, but not as high as coatings fabricated by EB–PVD or PS, due to the lower thickness of coatings deposited by sputtering (usually a few microns), so this technique is not commonly used alone for the deposition of commercial thermal barrier coatings. However, sputtered coatings can result interesting for example when good thermal insulting properties are desired together with strong corrosion resistance, thanks to the dense structure got in sputtered films and their strong adhesion aided by lower stresses deriving from the lower thickness [53].

For example, Amaya et al. [53] deposited 8 mol% Yttria-Stabilized Zirconia (8YSZ) by radio frequency (rf) magnetron sputtering as thermal barrier coating with also anticorrosion function on AISI-304 stainless steel. Prior to the YSZ growth, an Al/Al_2O_3 graded buffer layer was deposited to

improve the adhesion of the subsequent coating. The corrosion tests were conducted at temperature up to 700 °C in air and at exposure time up to 6 h, showing significant differences (one to three orders of magnitude) of corrosion resistance between the coated and uncoated steel.

Rösemann et al. in refs. [54,55] and their other works cited therein, studied the influence of different process parameters on the properties of fully and partially yttria-stabilized zirconia (8 mol% FYSZ and 4 mol% PYSZ, respectively) coatings for potential use in thermal barrier applications. In particular, they used the gas flow sputtering (GFS) technique, allowing higher deposition rates with respect to conventional magnetron sputtering, thus depositing coatings with thicknesses up to some tens of microns. The influence of different process parameters (bias voltage, oxygen flow rate, substrate temperature) was evaluated on the morphological, compositional and crystallographic properties of the grown films, and thermal cycling experiments were conducted between 100 °C and 1050 °C. In particular, a strong effect of the substrate temperature on the coating properties was found.

In a work by Noor-A-Alam et al. [56], coatings based on mixed hafnia and zirconia stabilized by yttria (Y_2O_3-stabilized HfO_2-ZrO_2, briefly YSHZ) were tested for TBC applications. Different coating compositions were studied by varying the relative concentration of HfO_2 and ZrO_2, at fixed Y_2O_3 stabilizer content of 7.5 mol%. The thermal stability of the YSHZ coatings was evaluated up to 1300 °C by XRD, SEM, and EDS analyses, showing no significant modifications of crystal structure, morphology and composition.

The use of other REOs like Gd_2O_3 as stabilizer in sputtered coatings based on zirconia with and without yttria was tested by Portinha et al. [57] as potential materials for TBCs. $ZrO_2Gd_2O_3$ and $ZrO_2Y_2O_3Gd_2O_3$ coatings were grown by DC magnetron sputtering at different compositions, with Gd_2O_3 content varying in the range from 6 to 38 wt.% in Gd_2O_3-stabilized ZrO_2, and Y_2O_3 and Gd_2O_3 contents in the respective ranges from 4 to 10 wt.% and from 11 to 20 wt.% in zirconia samples with both stabilizers. The zirconia phase was found to shift from tetragonal at lower stabilizers concentrations to cubic at increasing concentrations, while no significant changes were noticed in the coating morphology.

A summary of the sputtering parameters used in the works mentioned above are reported in Table 5.

Table 5. Deposition parameters, materials and film thicknesses for the coatings deposited by sputtering in the different works described in the text.

Coating Material	Deposition Technique	Coating Thickness	Target	Power	Process Pressure	Substrate Temperature	Bias Voltage	Reference
8YSZ	rf magnetron sputtering	~2.5 µm	YSZ	350 W	0.7 Pa (Ar)	300 °C	−20 V	[53]
8 mol% and 4 mol% YSZ	gas flow sputtering	~15–70 µm	ZrY alloy	5 kW (DC)	20–50 Pa (Ar + O_2)	500–800 °C	0–−100 V (pulsed DC)	[54,55] and works cited therein
YSHZ	sputtering	~1 µm	YSHZ	100 W	/(Ar)	500 °C	/	[56]
Gd_2O_3-stabilized ZrO_2 and Gd_2O_3-costabilized YSZ	DC magnetron sputtering	~1.2–3.8 µm	Zr doped with Gd and/or Y	Voltage 260–290 V	0.6 Pa (Ar + O_2)	250 °C	−50 V (DC)	[57]

In order to combine the strong adhesion characteristics of sputtered coatings together with the better thermal barrier properties induced by the thicker films deposited by plasma spray, the two techniques can be combined together in a multilayer structure, with the aim to reduce TBC failure due to coating spalling. To this aim, in [58] by Andritschky et al. a preliminary bond coat of yttria-partially-stabilized zirconia (PSZ, 8 µm thick) was deposited on the substrate by DC reactive magnetron sputtering, followed by a thicker PSZ coating (300 µm) deposited by plasma spray. Different thermal cycling tests were conducted on the analyzed coatings, showing no significant damage on the combined coatings under the experimental conditions used in the work.

A similar approach was used by Yao et al. [59], where a multilayered TBC was obtained by the combination of a bond coat layer deposited by sputtering and a top layer fabricated by EB–PVD, with the aim to improve the TBC performance thanks to reduced oxygen diffusion, inhibition of cracks propagation and stress relaxation, aided by the bond coat. In particular, a composite bond coat made of

Y_2O_3-doped Al_2O_3 and noble metals (Pt and Au) was grown on the substrate by depositing different alternating layers of Y_2O_3-doped Al_2O_3 (through rf magnetron sputtering from an Al_2O_3 target doped with 2 wt.% of Y_2O_3) and noble metal layers (through DC magnetron sputtering from a metal target), followed by thermal annealing, with a total thickness of about 1.4 μm. The subsequent 8YSZ top coat with thickness around 100 μm was then deposited on the bond coat by the EB–PVD process, and the combined coating was tested by high temperature cyclic oxidation tests at 1100 °C in air for 200 h. This composite coating showed strong adhesion on the substrate and resulted in a largely improved resistance to oxidation and spallation.

ZrYGdO coatings fabricated by cosputtering Y-and Gd-doped ZrO_2 targets were used as external barrier coatings on ion-plasma thermal barrier NiCrAlY (Re, Ta, Hf) + AlNiY (Hf) alloys and submitted to isothermal and cyclic heat-resistance tests. The effect of TBCs on the long-term strength at a test temperature of 1000 °C and on the high-cycle fatigue at 900 °C was investigated [60].

4. Perspectives for Using Zirconia Doped with Multicomponent Mixed REOs for TBC: Preliminary Results

From the critical analysis of the studies reported in the literature it is evident how the thermal properties of zirconia may be improved by using different rare earth oxides. The aim of the present work is to show the potential of using mixed rare earth oxides (REOs) as naturally occurring from monazite concentrates for obtaining stabilized ZrO_2 ceramic coatings for their potential used as TBCs.

Rare Earth Oxides naturally coexist in different ratios in concentrates such as monazite or bastnäsite. Their extraction, separation and purification in individual REOs is a process requiring special skills, hundreds of hydrometallurgical processing steps using organic solvent extraction, precipitation and calcination, with high environmental impact and energy consumption reflected in corresponding high prices. Despite the more and more theoretical and practical interest for using mixed REOs as dopants in high tech ceramics, only few attempts have been done to study the possibility to extract the naturally complex of REOs from concentrates and use them as multicomponent mixed doping oxides [61]. Here we present some preliminary results on the development of zirconia doped with multicomponent REOs simulating the composition from selected monazite concentrates after removal the radioactive elements (Th, U, and Ra). The aim is to further assess the potential use of naturally mixed REOs obtained directly from monazite concentrates.

Materials synthesis: In order to study the microstructure of mixed REOs-doped zirconia for potential applications in TBCs, five compositions of doped ZrO_2 powders have been obtained. In sample ZrO_2-RE1 the 8 wt.% Y_2O_3 usually employed as dopant for TBC was replaced with 8% synthetic REOs mixture with a ratio corresponding to natural occurrence in selected La-rich monazite concentrates. The other samples, denoted MxZy8La, MxZy8Sm, MxZy8Nd, and MxZy8Gd, represent ZrO_2 doped with 8 wt.% of each single element (La, Sm, Nd, and Gd, respectively), and were used as reference samples for the XRD analyses with the purpose to understand the XRD pattern of the REOs mixed co-doped powders.

All samples were prepared by a hydrothermal method at moderate temperatures (max. 250 °C) and pressures (max. 40 atm.). This method is characterized by three important advantages: improvement of the chemical reactivity, low energy consumption due to elimination of thermal treatment for crystallization, high homogeneity and control of nucleation and growth [62]. The synthesis was done from high purity raw materials: Y_2O_3 > 99%-Merck, La_2O_3 ≥ 99.9%-Roth, Nd_2O_3 ≥ 99.9%-Alfa Aesar, Sm_2O_3 ≥ 99.9%-Alfa Aesar, Gd_2O_3 ≥ 99.9%-Alfa Aesar and Yb_2O_3 99.9%-Alfa Aesar. Zirconium tetrachloride ($ZrCl_4$ 99% Merck) was used as raw material for preparing an aqueous Zr (IV) stock solution with programmed Zr concentration. The dissolution of REOs precursors in $ZrCl_4$ solution was done under vigorous mechanical stirring until a homogenous clear solution was obtained. Ammonia solution (NH_3 25% p.a., Chimreactiv srl) agent was added as mineralizing until an alkaline suspension with pH~9 was obtained. The doped powder was obtained by hydrothermal treatment in an autoclave (Berghof, Germany, TEFLON-linen, 5-L capacity, maximum operation temperature 250 °C, maximum

operating pressure 200 atm., endowed with water cooling system). The hydrothermal method used was described in [63]. The synthesis flowsheet is presented in Figure 1.

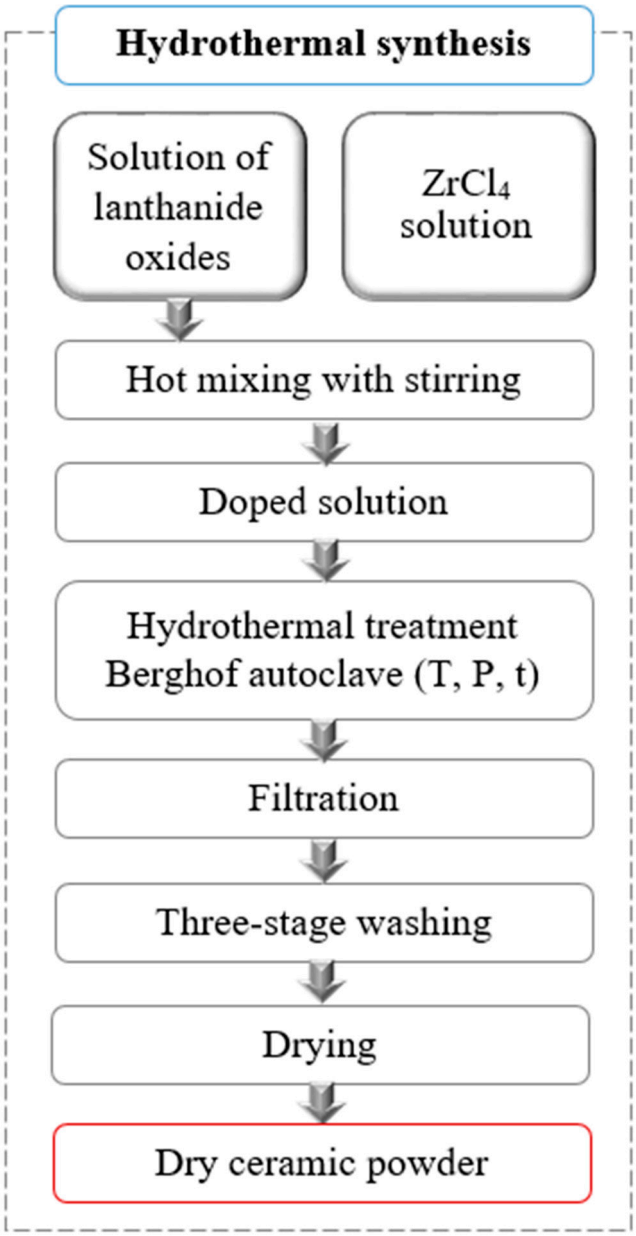

Figure 1. Schematic flowsheet of the hydrothermal process used for obtaining ZrO_2 powders doped with mixed rare earth oxides (REOs).

Spark plasma sintering (SPS) was used to achieve compacted materials virtually without porosity or bearing a minimal and almost insignificant porosity level [64]. All experiments were performed under a vacuum of 16.2 Pa with the pulse (3.3 ms) sequence for an applied voltage of 12:2 V (i.e., 12 ON/2 OFF). The samples were sintered at temperature of 1250 °C, for a dwell time of 20 min with heating and cooling rates of 10 °C/min. A known volume of 0.75 g of powder was used for each experiment. The experiment was carried out in a graphite mold with an inner diameter of 10 mm and an external diameter of 25 mm with internal diameter of the graphite die covered by flexible carbon foil (Papyex). The mold was covered with carbon fiber felt to limit the loss of heat radiation. The sintered pellets were used as source material for Electron-Beam Physical Vapor Deposition process.

Obtaining of mixed REOs-doped zirconia coatings. TB coatings were developed in a special designed EB–PVD thin film coating equipment (Torr International Inc., New Windsor, NY, USA) endowed with quartz sensors (QCM) mounted next to each crucible for monitoring the deposition rate and a software allowing the creation of complex deposition recipe that can be performed in automatic mode keeping constant the evaporation rate. The system is designed to combine multiple coatings, having 4 EB 10 KW power guns, each being equipped with four crucibles with body movement, allowing the continuous storage of 16 materials. The substrate material used was a high temperature NIMONIC 80A alloy in the form of sheets with sizes 30 mm × 50 mm, mounted on a heated support rotating at 20 rpm during coating process. All successive layers were deposited by EB–PVD process. Commercial NiCrAlY powders (Amperit) were used to deposit the bond coat prior to deposit the ceramic layer. Commercially $La_2Zr_2O_7$ (LZO) granulated powders (grain sizes 30–120 µm) and $Gd_2Zr_2O_7$ (GZO) granulated powders (grain sizes 45–140 µm) from Trans-Tech Ceramics and Advanced Materials USA were also used to deposit the outer layers, aiming to improve the thermal shock properties of the system. The schematic flowsheet of the whole process for obtaining mixed REOs doped ZrO_2 coatings is presented in Figure 2. The experimental parameters used for coating of sintered REOs-doped zirconia pellets are presented in Table 6.

Table 6. Working conditions and parameters.

Material Used and Number of Crucibles	Substrate Heating Temperature (°C)	Start Vacuum (Pa)	Working Vacuum (Pa)	Deposition Rate (Å/s)	Total Deposition Time (h)	Maximum Power (KW)
6 crucibles: 1*x*NiCrAlY 4 × ceramic pellets 1 × LZO, 1× GZO	650	1.33×10^{-4}	5.33×10^{-3}	0.8–1.4	57	10

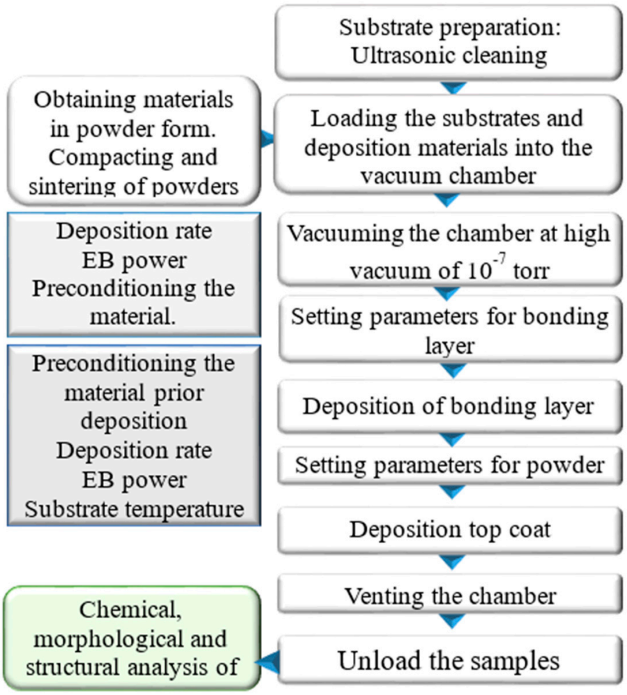

Figure 2. Schematic flowsheet for obtaining of mixed REO-doped ZrO_2 coatings.

Characterization methods: Chemical composition of REO-doped ZrO_2 was analyzed by Inductively Coupled Plasma-Optical Emission Spectrometry (Agilent 725 ICP-OES), according to ASTM E 1479-99(2011) standard. The microstructure of the as-obtained REO doped ZrO_2 powder was

examined using a BRUKER D8 ADVANCE X-ray diffractometer (Bruker AXS Company, Germany) with monochromatic Cu Kα radiation, Bragg–Brentano diffraction method. Scans were obtained in the 2θ range 4–74° with a step size of 0.02° every 2.5 or 6 s. For the identification of the phases contained in the samples, data processing was performed using software package DIFFRAC.SUITE.EVA release 2016 by Bruker AXS Company, Karlsruhe, Germany; SLEVE + 2020 and ICDD PDF-4 + 2020 database edited by International Centre for Diffraction Data (ICDD). X-ray diffraction analysis on the deposited thin films was performed using an Empyrean PANalytrical equipment in Bragg–Brentano geometry equipped with an in-focus Cu (λ Cu Kα = 1.541874 Å) X-ray tube, hybrid monochromator on the incident side and parallel plate collimator mounted on the detector a PIXcel3D on the diffracted side. The spectra were acquired in the 2θ range of 20–80°, with acquisition step of 0.02° and acquisition time per step of 4s. X-ray diffraction spectra have been processed in the specialized software HighScore Plus 3.0e software (PANalytical, Almelo, The Netherlands).

The morphology of the powder samples was investigated by scanning electron microscopy (SEM) using a high-resolution microscope Quanta 250 (FEI Company, Eindhoven, The Netherlands), incorporated with Energy Dispersive X-Ray Spectrometer, produced by EDAX (Mahwah, NJ, US), consisting of ELEMENT Silicon Drift Detector Fixed, Element EDS Analysis Software Suite APEX™ 1.0, EDAX, Mahwah, NJ, USA.

The characterization of the films by SEM-EDS was performed using the QUANTA INSPECT F50 SEM (FEI Company, Eindhoven, The Netherlands) equipped with field emission gun electron (FEG) with 1.2 nm resolution and energy dispersive X-ray spectrometer (EDS), with the resolution at MnK of 133 eV.

Roughness tests were developed using a digital roughness meter, INSIZE-ISR-C002 (type: Inductive; probe head material: diamond; measuring force: 4 mN; units: μm/min; number of interruptions: 1 to 5; crossing speed: 0.5 mms^{-1} and mms^{-1}; resolution (Ra): 0.001 μm).

The thermal shock test was performed with the help of a Quick Thermal Shock Installation (QTS-INCAS Bucharest, Romania), which has a maximum oven operating temperature of 1750 °C. The specimens were inserted into the oven by the action of a robot axis and kept in the oven for 5 min. The cooling stage is 60 s to reach the room temperature, which is produced by a jet of compressed air over a 5 mm nozzle at a pressure of 8 bar ± 10% at a distance of 45 mm from the sample under 45° degree of inclination. Temperature data are collected using 1 Pt/PtRh thermocouple inside the oven and 2 pyrometers outside the oven, for the temperature range −40–1750 °C. A pyrometer mounted on the oven monitors the temperature variation on the test tube inside the oven.

The chemical analysis of powders synthesized in hydrothermal conditions is presented in Table 7 and it is in accordance with the designed compositions. The XRD patterns of samples are presented in Figure 3. The quantitative phase analysis is presented in Table 8.

Table 7. Chemical composition of REO-doped ZrO_2 powders.

Sample		Chemical Analysis						
		La	Gd	Y	Yb	Sm	Nd	Zr
ZrO_2-RE1	wt.%	3.49	0.278	0.46	0.0032	0.409	2.33	52.19
MxZy8La	wt.%	8	-	5.50	-	<0.004	-	63.32
MxZy8Sm	wt.%	-	-	5.77	-	9.28		60.46
MxZy8Nd	wt.%	-	-	5.70	-	-	8.09	61.50
MxZy8Gd	wt.%	-	9.93	5.68	-	-	-	60.03

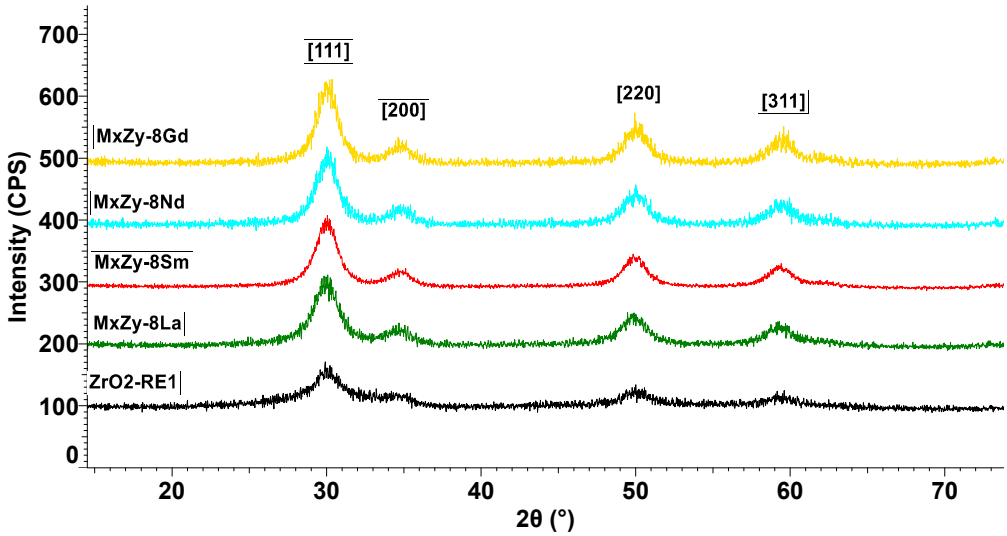

Figure 3. Diffraction spectrum for ZrO_2-RE1, MxZy8La, MxZy8Sm, MxZy8Nd, and MxZy8Gd samples.

Table 8. Quantitative phase analysis of ZrO_2 doped powders.

Sample	Major Phases	Formula	PDF File	Crystallization System
ZrO_2-RE1	Zirconium Yttrium Oxide	Solid solution	PDF 00-060-0505	Tetragonal
MxZy8La	Zirconium Yttrium Oxide type	Solid solution	PDF-01-077-2286	Cubic
	Baddeleyite	ZrO_2	PDF-00-036-0420	Monoclinic
MxZy8Sm	Zirconium Yttrium Oxide type	Solid solution	PDF 01-077-2286	Cubic
MxZy8Nd	Zirconium Yttrium Oxide type	Solid solution	PDF 01-077-2286	Cubic
MxZy8Gd	Zirconium Yttrium Oxide type	Solid solution	PDF 01-077-2286	Cubic
	Baddeleyite	ZrO_2	PDF 00-036-0420	Monoclinic

It may be observed that ZrO_2 doped with 8 wt.% La_2O_3, Sm_2O_3, and Nd_2O_3 are monophasic cubic solid solution, while ZrO_2 doped with 8 wt.% Gd_2O_3 consists of cubic solid solution as major phase and monoclinic ZrO_2 as minor phase. Sample ZrO_2-RE1 (composition simulating La-rich monazite concentrates) corresponds to a monophasic tetragonal ZrO_2 solid solution.

The morphology of these powders is presented in Figure 4. All hydrothermally synthesized powders consist of granular aggregates with dimensions up to tens of microns. EDS analysis (not shown) confirms the presence of REOs doping elements uniformly distributed in the aggregates.

Different coatings architectures were obtained from ZrO_2-RE1 pellets, LZO and GZO granulated powders. The section view of a typical architecture of EB–PVD coatings on Nimonic 80 A substrate (Figure 5) highlights the presence of the 4 layers arranged as follows: NiCrAlY bonding layer with 0.556 ± 0.072 µm thickness, YSZ with 1.984 ± 0.151 µm layer thickness, LZO layer thickness 4.245 ± 0.119 µm and GZO with a layer thickness of 4.618 ± 0.191 µm. The total thickness of the deposit is around 11.50 µm. Elemental mapping, through the colors chosen for the specific elements, confirms the clear limits of each layer.

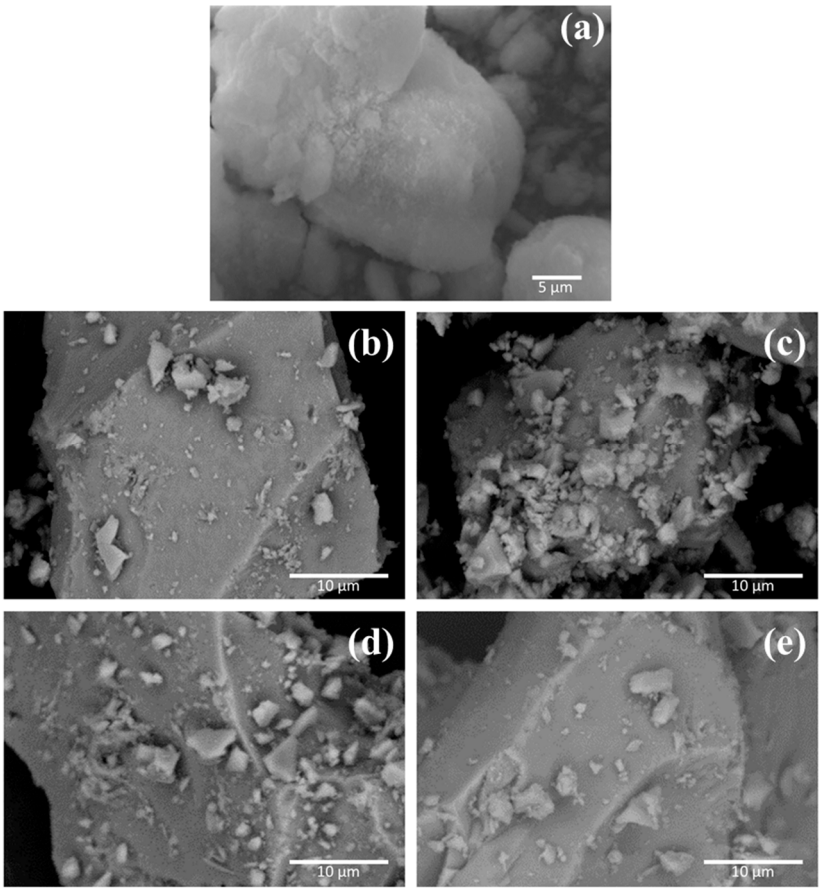

Figure 4. Scanning electron microscopy (SEM Quanta 250 FEI Company, Eindhoven, The Netherlands) images for samples: (**a**) ZrO2-RE1; (**b**) MxZy8La; (**c**) MxZy8Sm; (**d**) MxZy8Nd; and (**e**) MxZy8Gd.

SEM analysis on the coated surface (Figure 5a) shows that the deposition is uniform with a continuous film on the substrate. Polyhedral grains with well-defined edges and dimensions between 190 and 380 nm are identified.

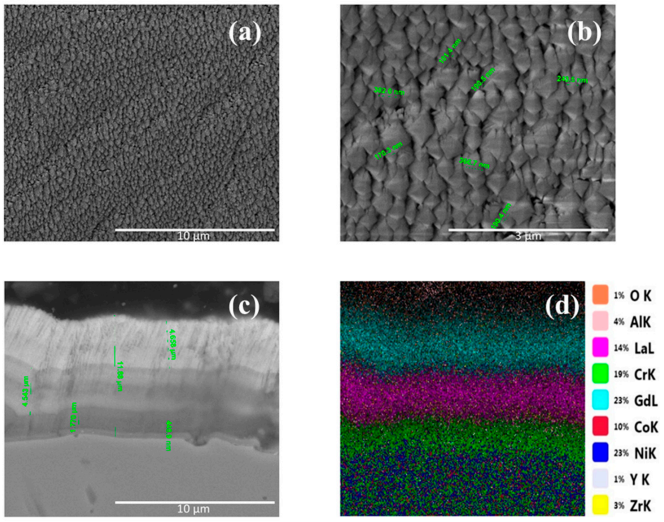

Figure 5. SEM images (50,000×), QUANTA INSPECT F50, FEI Company, Eindhoven, The Netherlands, representing: (**a**) and (**b**) the surface of the NiCrAlY/YSZ/LZO/GZO coating deposited on Nimonic substrate at different magnifications; (**c**) the section view of NiCrAlY/ZrO2-RE1/LZO/GZO type deposition on Nimonic substrate, and (**d**) the elemental mapping.

In Figure 6, the XRD spectrum of the Nimonic 80 A coated with four layers of material (NiCrAlY/YSZ/LZO/GZO) is presented, showing the presence of $Gd_2Zr_2O_7$ (ICDD PDF4 + 01-078-4083) and $La_2Zr_2O_7$ (ICDD PDF4 + 00-050-0837). The presence of REOs doped ZrO_2 solid solution cannot be observed, due to the attenuation of the X-ray radiation by the upper layers.

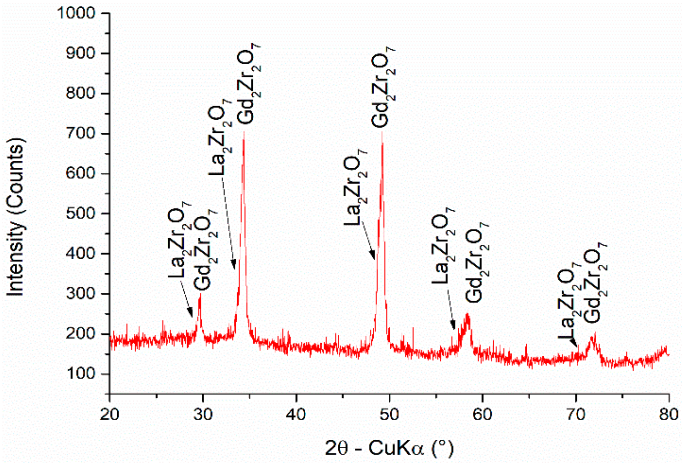

Figure 6. X-ray diffraction spectrum obtained for Nimonic with 4 layers of material (NiCrAlY/ZrO2-RE1/LZO/GZO).

The Nimonic sample coated with four layers of NiCrAlY/ZrO_2-RE1/LZO/GZO material was subjected to heat treatment at a temperature of 1250 °C for 10 min in nitrogen to determine its behavior under high temperature conditions. The SEM micrographs obtained after treatment are shown in Figure 7. One can observe in Figure 7b and from the corresponding map (Figure 7d), that during heat treatment, most probably during cooling in air, the substrate/bondcoat became oxidized, showing typical oxide scale morphology between substrate and ceramic coating and enrichment of Cr, most probably with the formation of Cr_2O_3 oxide. Small cracks appear at the intergranular boundaries in the ZrO_2-REO1 layer and the diffusion of Ti and Cr from the substrate towards the cracking layer, as well as the formation of TiO_2 were observed.

The corresponding XRD spectrum of the coating after the heat treatment (Figure 8) shows the presence of $Gd_2Zr_2O_7$ (ICDD PDF4 + 01-078-4083) and $La_2Zr_2O_7$ (ICDD PDF4 + 00-050-0837) phases, while the presence of ZrO_2-RE1 and other secondary phases formed at the substrate/ceramic layer interface is hindered.

From the roughness investigations results presented in Figure 9, a slight change in the mean surface roughness from 0.448 μm of the Nimonic 80A substrate to 0.521 μm for the coated Nimonic substrate may be observed. These values are very similar, thus proving that the coatings grow uniformly following the substrate morphology.

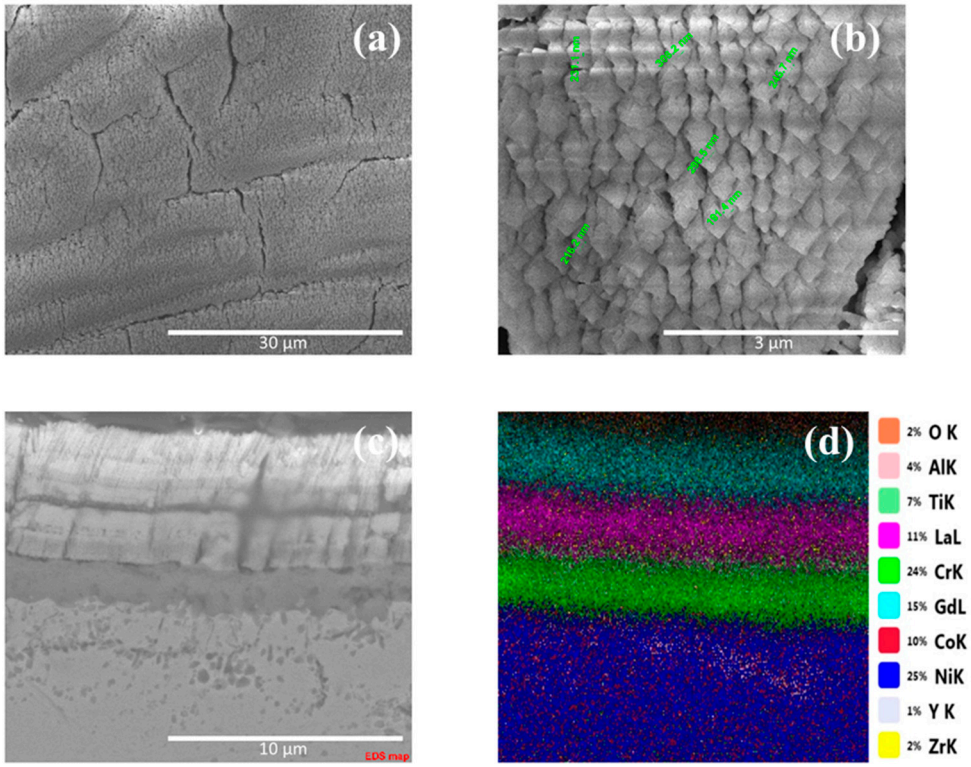

Figure 7. SEM images (QUANTA INSPECT F50, FEI Company, Eindhoven, The Netherlands) representing (**a**) and (**b**) the surface of the NiCrAlY/ZrO2-RE1/LZO/GZO multilayer coating on the Nimonic substrate after heat treatment at 1250 °C (40,000×); (**c**) cross section of the NiCrAlY/ZrO2-RE1/LZO/GZO on Nimonic substrate; and (**d**) elemental mapping after heat treatment.

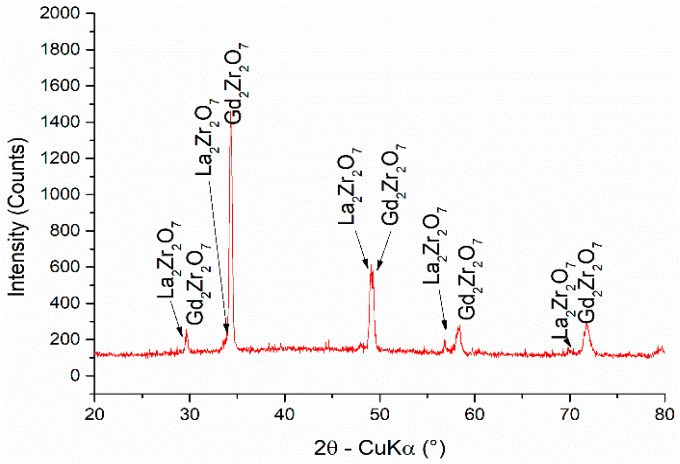

Figure 8. X-ray diffraction spectrum obtained for Nimonic with 4 layers of material (NiCrAlY/YSZ/LZO/GZO) after heat treatment at 1250 °C.

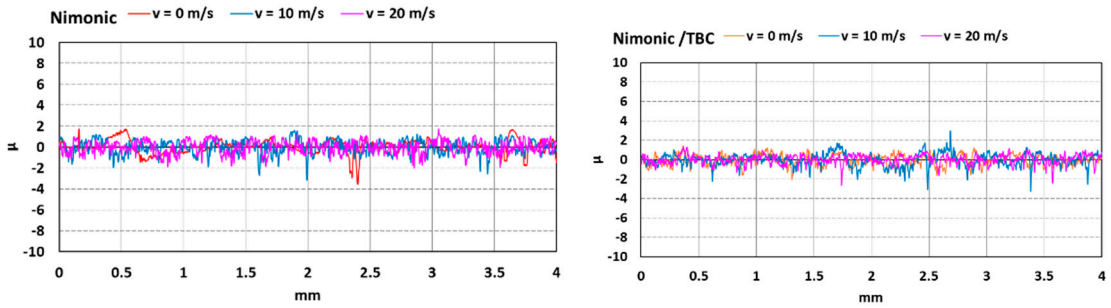

Figure 9. Surface roughness investigations of uncoated and coated Nimonic 80A substrate.

The results of thermal shock tests are presented in Figures 10 and 11. This test shows the number of heating and cooling cycles that a coated material may support without delamination of the coating layers. Comparison between thermal shock values of new coatings architecture with existing ones may be a method to assess their potential application in aeronautics. The results show a satisfactory behavior obtained after a number of minimum 150 cycles in the temperature ranges 1200−1300 °C for the proposed NiCrAlY/ZrO2-RE1/LZO/GZO coating architecture with a total thickness of about 11.5 μm. The results are comparable with those of traditional YSZ coatings with thickness greater than 100 μm [65], showing the ability of the new coating materials to further improve the thermal properties of TBCs for aeronautical applications at much lower thickness.

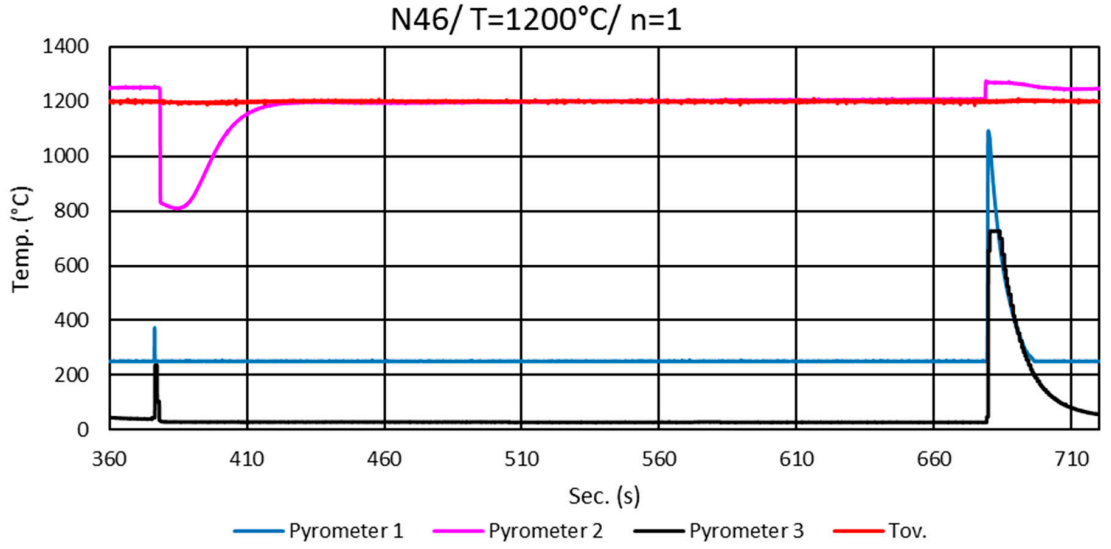

Figure 10. Thermal shock tests. The red line (TCup)—represents the recorded temperature of the oven by the Pt/PtRh thermocouple mounted inside the oven; magenta line (Pyrometer 2) represents the temperature of the sample over the heating stage during the test, which shows a peak starting from low temperature and a stabilized temperature for dwell time. The blue and black lines represent the temperature change of the sample over the cooling stage by Pyrometer 1 and Pyrometer 3, respectively.

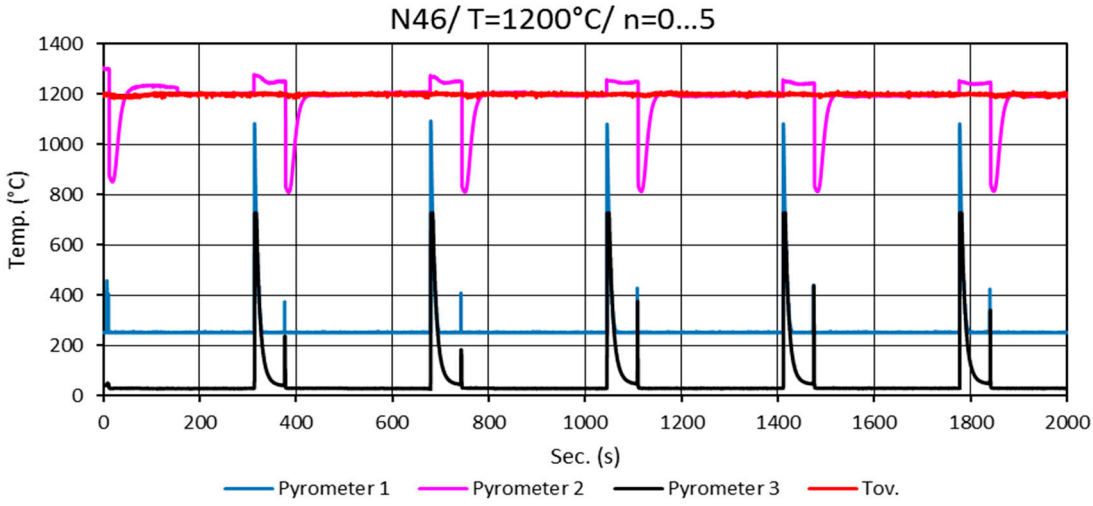

Figure 11. Thermogram for thermal shock cycles 38–43, temperature range 800–1300 °C.

5. Conclusions and Future Prospects

During recent years, it was demonstrated that co-doping of zirconia ceramics with REOs may avoid grain size coarsening due to interface segregation, enhancing its ionic conductivity and sinterability. ZrO_2 doped with 7–8 wt.% Y_2O_3 (8YSZ) are presently considered as a "gold standard" in coating materials for TBC applications. New TBCs that can operate at a temperature above 1200 °C are needed and doping ZrO_2 ceramics with mixed rare earth oxides is a possible solution due to the high temperature transformation and the low thermal conductivity. The influence of the synthesis route on the microstructure and properties of ZrO_2 doped with different REOs mixed compositions are presented and discussed.

Rare-earth zirconates with perovskite or pyrochlore structure are also considered as emerging TBC materials for the future, due to their stability up to the melting point, low intrinsic thermal conductivity, associated with the complexity of crystallographic structure and large quantities of oxygen ion vacancies.

Different physical vapor deposition methods have been proposed to obtain TBCs from these high temperature oxides. EB–PVD method was largely used to obtain coatings with desired properties for aeronautics and energy generation systems due to the specific columnar growth and good adhesion to the substrate.

In this paper, we presented some preliminary results on the development of zirconia doped with multicomponent REOs simulating the composition existing in some selected monazite concentrates after removal of the radioactive elements (Th, U, and Ra). The aim is to further assess the potential use of naturally mixed REOs obtained directly from monazite concentrates. ZrO_2 powders doped with 8% synthetic REOs mixture (containing La, Gd, Y, Nd, Gd, and Yb with a ratio corresponding to natural occurrence in selected La-rich monazite concentrates) have been prepared by a hydrothermal method at moderate temperatures (max. 250 °C) and pressures (max. 40 atm.). The XRD pattern of this powder corresponds to a monophasic tetragonal ZrO_2 solid solution, consisting of granular aggregates with dimensions up to tens of microns. EDS analysis confirms the presence of REOs doping elements uniformly distributed in the aggregates.

Coatings architectures deposited on Nimonic 80 A substrates were further obtained using these powders, consisting of NiCrAlY bonding layer with 556 nm thickness, YSZ with 1.98 µm layer thickness, LZO layer thickness 4.25 µm and GZO with a layer thickness of 4.62 µm. The results of thermal shock tests show a satisfactory behavior for a number of minimum 150 cycles in the temperature ranges 1200−1300 °C for the proposed coating architecture with a total thickness around 11.5 µm. The results are comparable with those of traditional YSZ coatings with thickness >100 µm, showing the ability of the new coating materials to further improve the thermal properties of TBCs for aeronautical applications.

Works are under progress to obtain TBC coatings based on ZrO_2 doped with synthetic REOs mixtures simulating Ce-rich monazite concentrates. The results will be further compared to those obtained using natural mixed REOs obtained from monazite concentrates, to assess the possibility to use them as dopants and demonstrate their economic impact in aeronautics and energy generation.

Author Contributions: Conceptualization, R.R.P.; methodology, M.C. and M.P.; validation, A.M.M. and V.D.; formal analysis, B.S.V.; investigation, M.B., A.V.S. and R.T.; resources, S.V.; data curation, A.E.S.; writing—original draft preparation, A.E.S., D.V., M.L.G. and R.R.P.; writing—review and editing, D.V. and M.L.G.; supervision, R.R.P. and M.L.G. All authors have read and agreed to the published version of the manuscript.

Funding: This research was funded by H2020 ERAMIN II Programme, MONAMIX project ID 87, financed in the frame of grant 50/2018 UEFISCDI Romania, Ctr. ANR-17-MIN2-0003-03 France and Ctr. MIUR 8361/05 May 2017-CUP n. B86G17000750001 Italy. Mircea Corban acknowledges the funding in the frame of project PN 19 19 04 01 financed by Romanian Ministry for Education and Research. Mihai Botan akcnowledges the funding by the European Social Fund through the Sectoral Operational Programme Human Capital 2014–2020, through the Financial Agreement with the title "Scholarships for entrepreneurial education among doctoral students and postdoctoral researchers", Acronym Be Entrepreneur!, Contract no. 51680/09.07.2019-SMIS code: 124539.

Acknowledgments: Radu R. Piticescu, Maria Luisa Grilli, Daniele Valerini and Mythili Prakasam acknowledge also the networking support from COST Action CA 15102 CRM Extreme (2016–2020) and CIG−15102 ITHACA (2020–2021).

Conflicts of Interest: The authors declare no conflict of interest.

References

1. Darolia, R. Thermal barrier coatings technology: Critical review, progress update, remaining challenges and prospects. *Int. Mater. Rev.* **2013**, *58*, 315–348. [CrossRef]
2. Castro, J.; Nafsin, N.J. Direct measurements of quasi-zero grain boundary energies in Ceramics. *J. Mater. Res.* **2017**, *32*, 166–173.
3. Dragut, D.V.; Badilita, V.; Motoc, A.M.; Piticescu, R.R.; Zhao, J.; Hijji, H.; Conte, L. Thermal stability and field assisted sintering of cerium-doped YSZ ceramic nanoparticles obtained via a hydrothermal process. *Manuf. Rev.* **2017**, *4*, 11. [CrossRef]
4. Sobetkii, A.; Rinaldi, A.; Cuesta-Lopez, S.; Prakasam, M.; Largeteau, A.; Plaiasu, G.; Piticescu, R.R. Novel high temperature oxide ceramic coatings: Synthesis, properties and applications. In Proceedings of the International Conference FiMPART, Bordeaux, France, 9−12 July 2017.
5. Ekström, M.; Thibblin, A.; Tjernberg, A.; Blomqvist, C.; Jonsson, S. Evaluation of internal thermal barrier coatings for exhaust manifolds. *Surf. Coat. Technol.* **2015**, *272*, 198–212. [CrossRef]
6. Patnaik, P.; Huang, X.; Singh, J. State of the Art and Future Trends in the Development of Thermal Barrier Coating Systems. In *Innovative Missile Systems*; Meeting Proceedings RTO-MP-AVT−135, Paper 38; RTO: Neuilly-sur-Seine, France, 2006; Volume 38, p. 20.
7. Boke, Y.E.; Altun, O. Heat transfer analysis of thermal barrier coatings on a metal substrate. *J. Therm. Sci. Technol.* **2013**, *33*, 101–109.
8. Mehdi, K.; Soheil, N. The evolution of fracture process zones in as-received and oxidized air. *Surf. Coat. Technol.* **2019**, *377*, 124885.
9. Kadir, M.D.; Yasin, O.; Hayrettin, A.; Abdullah, C.K. Evaluation of oxidation and thermal cyclic behavior of YSZ. Gd2Zr2O7 and YSZ/Gd2Zr2O7 TBCs. *Surf. Coat. Technol.* **2019**, *371*, 262–275.
10. Lei, G.; Chenglong, Z.; Mingzhu, L.; Wei, S.; Zhaoyang, Z.; Fuxing, Y. Hot corrosion evaluation of Gd_2O_3-Yb_2O_3 co-doped Y_2O_3 stabilized ZrO_2 thermal barrier oxides exposed to Na_2SO_4 + V_2O_5 molten salt. *Ceram. Int.* **2017**, *43*, 2780–2785.
11. Cao, X.; Vassen, R.; Stoever, D. Ceramic Materials for Thermal Barrier Coatings. *J. Eur. Ceram. Soc.* **2004**, *24*, 1–10. [CrossRef]
12. Venkatesh, G.; Subramanian, R.; John Berchmans, L. Phase Analysis and Microstructural Investigations of Ce2Zr2O7 for High-Temperature Coatings on Ni-Base Superalloy Substrates. *High Temp. Mater. Proc.* **2019**, *38*, 773–782. [CrossRef]
13. Bahamirian, M.; Hadavi, S.M.M.; Farvizia, M.; Rahimipoura, M.R.; Keyvanic, A. Phase stability of ZrO2 9.5Y2O3 5.6Yb2O3 5.2Gd2O3 compound at 1100 °C and 1300 °C for advanced TBC applications. *Ceram. Int.* **2019**, *45*, 7344–7350. [CrossRef]

14. Miller, R.A. Thermal Barrier Coatings for Aircraft Engines: History and Directions. *J. Therm. Spray Technol.* **1997**, *6*, 35. [CrossRef]
15. Prakasam, M.; Valsan, S.; Lu, Y.; Balima, F.; Lu, W.; Piticescu, R.; Largeteau, A. Nanostructured Pure and Doped Zirconia: Syntheses and Sintering for SOFC and Optical Applications. *Sinter. Technol. Method Appl.* **2018**, 85. [CrossRef]
16. Ultramet Advanced Materials Solutions. Available online: https://ultramet.com/ceramic-protective-coatings/refractory-oxides/ (accessed on 29 May 2020).
17. Dong, T.S.; Wang, R.; Di, Y.L.; Wang, H.D.; Lia, G.L.; Fu, B.G. Mechanism of high temperature oxidation resistance improvement of double-layer thermal barrier coatings (TBCs) by La. *Ceram. Int.* **2019**, *45*, 9126–9135. [CrossRef]
18. Zhou, S.; Shen, S.; Fang, X.; Hou, Q.; Zhao, D. An accurate and rapid method to compare thermal insulation capacity of nine Gd-Yb-YSZ coatings. *Ceram. Int.* **2019**, *45*, 19910–19917. [CrossRef]
19. Boissonnet, G.; Chalk, C.; Nicholls, J.; Bonnet, G.; Pedraza, F. Thermal insulation of CMAS (CalciumMagnesium-Alumino-Silicates)- attacked plasma-sprayed thermal barrier coatings. *J. Eur. Ceram. Soc. Elsevier* **2020**, *40*, 2042–2049. [CrossRef]
20. Sasikumar, K.; Bharathikannan, R.; Raja, M.; Mohanbabu, B. Fabrication and characterization of rare earth (Ce. Gd, and Y) doped ZrO2 based metal-insulator-semiconductor (MIS) type Schottky barrier diodes. *Superlattices Microstruct.* **2020**, *139*, 106424. [CrossRef]
21. Mekala, R.; Deepa, B.; Rajendran, V. Preparation. characterization and antibacterial property of rare earth (Dy and Ce) doping on ZrO2 nanoparticles prepared by co-precipitation method. *Mater. Today Proc.* **2018**, *5*, 8837–8843. [CrossRef]
22. Deng, J.; Li, S.; Xiong, L.; Wang, J.; Yuan, S.; Chen, Y. Different thermal behavior of nanostructured CeO_2-ZrO_2 based oxides with varied Ce/Zr molar ratios. *Mater. Chem. Phys.* **2019**, *236*, 121767. [CrossRef]
23. Madhusudhanaa, H.C.; Shobhadevic, S.N.; Nagabhushanad, B.M.; Hari Krishnad, R.V.; Murugendrappa, M.; Nagabhushanaf, H. Structural Characterization and Dielectric studies of Gd doped ZrO_2 nano crystals Synthesized by Solution combustion method. *Mater. Today Proc.* **2018**, *5*, 21195–21204. [CrossRef]
24. Xiao, D.Q.; He, G.J.; Lv, G.P.; Wang, H.; Liu, M.; Gao, J.; Jin, P.; Jiang, S.S.; Li, W.D.; Sun, Z.Q. Interfacial modulation and electrical properties improvement of solution-processed ZrO_2 gate dielectrics upon Gd incorporation. *J. Alloy. Compd.* **2017**, *699*, 415–420. [CrossRef]
25. Guo, L.; Li, M.; Ye, F. Phase stabilityandthermalconductivityof RE_2O_3 (RE$\frac{1}{4}$La. Nd, Gd, Yb) and Yb_2O_3 co-doped Y_2O_3 stabilized ZrO_2 ceramics. *Ceram. Int.* **2016**, *42*, 7360–7365. [CrossRef]
26. Song, X.; Xie, M.; Mub, R.; Zhou, F.; Jia, G.; An, S. Influence of the partial substitution of Y_2O_3 with Ln_2O_3 (Ln = Nd, Sm, Gd) on the phase structure and thermophysical properties of ZrO_2–Nb_2O_5–Y_2O_3 ceramics. *Acta Mater.* **2011**, *59*, 3895–3902. [CrossRef]
27. Song, X.; Xie, M.; An, S.; Hao, X.; Mu, R. Structure and thermal properties of ZrO_2–Ta_2O_5–Y_2O_3–Ln_2O_3 (Ln = Nd. Sm or Gd) ceramics for thermal barrier coatings. *Scr. Mater.* **2010**, *62*, 879–882. [CrossRef]
28. Mikhailov, D.A.; Orlova, A.I.; Malanina, N.V.; Nokhrin, A.V.; Potanina, E.A.; Chuvil'deev, V.N.; Boldin, M.S.; Sakharov, N.V.; Belkin, O.A.; Kalenova, M.Y.; et al. A study of fine-grained ceramics based on complex oxides ZrO_2-Ln_2O_3 (Ln= Sm, Yb) obtained by Spark Plasma Sintering for inert matrix fuel. *Ceram. Int.* **2018**, *44*, 18595–18608. [CrossRef]
29. Wang, Y.; Chen, L.; Feng, J. Impact of ZrO_2 alloying on thermo-mechanical properties of Gd_3NbO_7. *Ceram. Int.* **2020**, *46*, 6174–6181. [CrossRef]
30. Chen, C.; Liang, T.; Guo, Y.; Chena, X.; Man, Q.; Zhang, X.; Zeng, J.; Ji, V. Effect of scandia content on the hot corrosion behavior of Sc_2O_3 and Y_2O_3 co-doped ZrO_2 in Na_2SO_4+V_2O_5 molten salts at 1000 °C. *Corros. Sci.* **2019**, *158*, 108094. [CrossRef]
31. Pitek, F.M.; Levi, C.G. Opportunities for TBCs in the ZrO_2–$YO_{1.5}$–$TaO_{2.5}$ system. *Surf. Coat. Technol.* **2007**, *201*, 6044–6050. [CrossRef]
32. Fan, W.; Baia, Y.; Wang, Z.Z.; Che, J.W.; Wang, Y.; Tao, W.Z.; Wang, R.J.; Liang, G.Y. Effect of point defects on the thermal conductivity of Sc_2O_3-Y_2O_3 costabilized tetragonal ZrO_2 ceramic materials. *J. Eur. Ceram. Soc.* **2019**, *39*, 2389–2396. [CrossRef]
33. Sun, L.; Guon, H.; Peng, H.; Gong, S.; Xu, H. Influence of partial substitution of Sc_2O_3 with Gd_2O_3 on thephase stability andthermalconductivityof$Sc2O_3$-doped ZrO_2. *Ceram. Int.* **2013**, *39*, 3447–3451. [CrossRef]

34. Fabrichnaya, O.; Wang, C.; Zinkevich, M.; Levi, C.G.; Aldinger, F.J. Phase equilibria and thermodynamic properties of the ZrO_2-$GdO_{1.5}$-$YO_{1.5}$ system. *J. Phase Equilib. Diff.* **2005**, *26*, 591–604. [CrossRef]
35. Fabrichnaya, O.; Savinykh, G.; Zienert, T.; Schreiber, G.; Seifert, H.J. Phase relations in the ZrO_2-Sm_2O_3-Y_2O_3-Al_2O_3 system: Experimental investigation and thermodynamic modelling. *Int. J. Mater. Res.* **2012**, *103*, 1469–1487. [CrossRef]
36. Andrievskaya, E.R.; Samelyuk, A.V.; Lopato, L.M. Reaction of cerium oxide with zirconium and yttrium oxides at 1250 °C. *Powder Metall. Met. Ceram.* **2002**, *41*, 63–71. [CrossRef]
37. Longo, V.; Podda, L. Relazioi tra le fasi allo stato solido nel sistema CeO_2–ZrO_2–Y_2O_3 tra 1700 e 1400 °C. *Ceramica (Florence)* **1984**, *37*, 18–20.
38. Li, L.; Van der Biest, O.; Wang, P.L.; Vleugels, J.; Chen, W.W. Estimation of the phase diagram for the ZrO2-Y2O3-CeO2 system. *J. Eur. Ceram. Soc.* **2001**, *21*, 2903–2910. [CrossRef]
39. Fabrichnaya, O.B.; Savinykh, G.; Schreiber, G.; Dopita, M.; Seifert, H.J. Experimental investigation and thermodynamic modelling in the ZrO_2–La_2O_3–Y_2O_3 system. *J. Alloys Compd.* **2010**, *493*, 263–271. [CrossRef]
40. Fabrichnaya, O.B.; Savinykh, G.; Schreiber, G.; Seifert, H.F. Phase relations in the ZrO_2 –Nd_2O_3 –Y_2O_3 system: Experimental study and CALPHAD assessment. *Int. J. Mater. Res.* **2010**, *101*, 1354–1360. [CrossRef]
41. Zhang, D.; Gong, S.; Huibin, X. Thermal cycling behaviors of thermal barrier coatings on intermetallic Ni3Al based superalloy. *Surf. Coat. Technol.* **2003**, *168*, 78–83. [CrossRef]
42. Boissonnet, G.; Chalk, C.; Nicholls, J.R.; Bonnet, G.; Pedraza, F. Phase stability and thermal insulation of YSZ and erbia-yttria co-doped zirconia EB–PVD thermal barrier coating systems. *Surf. Coat. Technol.* **2020**, *389*, 125566. [CrossRef]
43. Cao, X.; Vassen, R.; Jungen, W.; Schwartz, S.; Tietz, F.; Stöver, D. Thermal stability of lanthanum zirconate plasma-sprayed coating. *J. Am. Ceram. Soc.* **2001**, *84*, 2086–2090. [CrossRef]
44. Vassen, R.; Cao, X.Q.; Tietz, F.; Basu, D.; Stöver, D. Zirconates as new materials for thermal barrier coatings. *J. Am. Ceram. Soc.* **2000**, *83*, 2023–2028. [CrossRef]
45. Mercer, C.; Williams, J.R.; Clarke, D.R.; Evans, A.G. On a ferroelastic mechanism governing the toughness of metastable tetragonal-prime (t′) yttria-stabilized zirconia. *Proc. R. Soc. A* **2007**, *463*, 1393–1408. [CrossRef]
46. Guo, X.Y.; Li, L.; Park, H.M.; Knapp, J.; Jung, Y.G.; Zhang, J. Mechanical properties of layered $La_2Zr_2O_7$ thermal barrier coatings. *J. Therm. Spray Technol.* **2018**, *27*, 1–10. [CrossRef]
47. Zhang, D.; Liao, K.; Yu, Y.; Tian, Z.; Cao, Y. Microstructure and thermal & mechanical properties of La2Zr2O7@YSZ composite ceramic. *Ceram. Int.* **2020**, *46*, 4737–4747.
48. Karaoglanli, A.C.; Doleker, K.M.; Ozgurlu, Y. Interface failure behavior of yttria stabilized zirconia (YSZ), $La_2Zr_2O_7$, $Gd_2Zr_2O_7$, YSZ/$La_2Zr_2O_7$ and YSZ/$Gd_2Zr_2O_7$ thermal barrier coatings (TBCs) in thermal cyclic exposure. *Mater. Charact.* **2020**, *159*, 110072. [CrossRef]
49. Doleker, K.M.; Ozgurluk, Y.; Karaoglanl, A.C. Isothermal oxidation and thermal cyclic behaviors of YSZ and doublelayered YSZ/La2Zr2O7 thermal barrier coatings (TBCs). *Surf. Coat. Technol.* **2018**, *351*, 78–88. [CrossRef]
50. Naga, S.M.; Awaad, M.; El-Maghraby, H.F.; Hassan, A.M.; Elhoriny, M.; Killinger, A.; Gadow, R. Effect of La2Zr2O7 coat on the hot corrosion of multi-layer thermal barrier coatings. *Mater. Des.* **2016**, *102*, 1–7. [CrossRef]
51. Wang, C.; Wang, Y.; Fan, S.; You, Y.; Wang, L.; Yang, C. Optimized functionally graded La_2Zr_2O/8YSZ thermal barrier coatings. *J. Alloy. Compd.* **2015**, *649*, 1182–1190. [CrossRef]
52. Ozgurluk, Y.; Doleker, K.M.; Karaoglanli, A.C. Hot corrosion behavior of YSZ, $Gd_2Zr_2O_7$ and YSZ/$Gd_2Zr_2O_7$ thermal barrier coatings exposed to molten sulfate and vanadate salt. *Appl. Surf. Sci.* **2018**, *438*, 96–113. [CrossRef]
53. Amaya, C.; Aperador, W.; Caicedo, J.C.; Espinoza-Beltrán, F.J.; Muñoz-Saldaña, J.; Zambrano, G.; Prieto, P. Corrosion study of Alumina/Yttria-Stabilized Zirconia (Al_2O_3/YSZ) nanostructured Thermal Barrier Coatings (TBC) exposed to high temperature treatment. *Corros. Sci.* **2009**, *51*, 2994. [CrossRef]
54. Rösemann, N.; Ortner, K.; Petersen, J.; Schadow, T.; Bäker, M.; Bräuer, G.; Rösler, J. Influence of bias voltage and oxygen flow rate on morphology and crystallographic properties of gas flow sputtered zirconia coatings. *Surf. Coat. Technol.* **2015**, *276*, 668.
55. Rösemann, N.; Ortner, K.; Bäker, M.; Petersen, J.; Bräuer, G.; Rösler, J. Influence of the Oxygen Flow Rate on Gas Flow Sputtered Thermal Barrier Coatings. *J. Ceram. Sci. Technol.* **2018**, *9*, 29.
56. Noor-A-Alam, M.; Choudhuri, A.R.; Ramana, C.V. Effect of composition on the growth and microstructure of hafnia–zirconia based coatings. *Surf. Coat. Technol.* **2011**, *206*, 1628. [CrossRef]

57. Portinha, A.; Teixeira, V.; Carneiro, J.; Costa, M.F.; Barradas, N.P.; Sequeira, A.D. Stabilization of ZrO_2 PVD coatings with Gd_2O_3. *Surf. Coat. Technol.* **2004**, *107*, 188–189. [CrossRef]
58. Andritschky, M.; Teixeira, V.; Rebouta, L.; Buchkremer, H.P.; Stover, D. Adherence of combined physically vapor-deposited and plasma-sprayed ceramic coatings. *Surf. Coat. Technol.* **1995**, *101*, 76–77.
59. Yao, J.; He, Y.; Wang, D.; Peng, H.; Guo, H.; Gong, S. Thermal barrier coatings with (Al_2O_3–Y_2O_3)/(Pt or Pt–Au) compositebond coat and 8YSZ top coat on Ni-based superalloy. *Appl. Surf. Sci.* **2013**, *286*, 298. [CrossRef]
60. Budinovskiia, S.A.; Matveeva, P.V.; Smirnova, A.A.; Chubarov, D.A. Thermal-Barrier Coatings with an External Magnetron-Sputtered Ceramic Layer for High-Temperature Nickel Alloy Turbine Blades. *Russ. Metall. (Met.)* **2019**, *6*, 617–623. [CrossRef]
61. Tabatabaeian, M.R.; Rahmanifard, R.; Jalili, Y.S. The study of phase stability and thermal shock resistance of a Scandia–Ceria stabilized zirconia as a new TBC material. *Surf. Coat. Technol.* **2019**, *374*, 752–762. [CrossRef]
62. Byrappa, K.; Yoshimura, M. *Handbook of Hydrothermal Technology*, 2nd ed.; Elsevier: Amsterdam, The Netherlands, 2013.
63. Piticescu, R.R.; Corban, M.; Grilli, M.L.; Balima, F.; Prakasam, M. Design of new coatings and sintered materials based on mixed rare earth oxides. *J. Nucl. Res. Dev.* **2019**, *18*, 18–23.
64. Piticescu, R.R.; Malic, B.; Kosec, M.; Motoc, A.; Monty, C.; Soare, I.; Kosmac, T.; Daskobler, A. Synthesis and sintering behaviour of hydrothermally synthesized YTZP nanopowders for ion-conduction applications. *J. Eur. Ceram. Soc.* **2004**, *24*, 1941–1944. [CrossRef]
65. Ionescu, G.; Manoliu, V.; Alexandrescu, E.; Stefan, A.; Mihailescu, A. The behavior of multilayer ceramic protecting at thermal shock. *Incas Bull.* **2013**, *5*, 25–32.